



## Operating point dependent variable switching point predictive current control for PMSM drives

### Citation

Wendel, S., Karamanakos, P., Dietz, A., & Kennel, R. (2019). Operating point dependent variable switching point predictive current control for PMSM drives. In *PRECEDE 2019: 2019 IEEE International Symposium on Predictive Control of Electrical Drives and Power Electronics* (pp. 1-6). IEEE.  
<https://doi.org/10.1109/PRECEDE.2019.8753362>

### Year

2019

### Version

Peer reviewed version (post-print)

### Link to publication

[TUTCRIS Portal \(http://www.tut.fi/tutcris\)](http://www.tut.fi/tutcris)

### Published in

PRECEDE 2019

### DOI

[10.1109/PRECEDE.2019.8753362](https://doi.org/10.1109/PRECEDE.2019.8753362)

### Take down policy

If you believe that this document breaches copyright, please contact [cris.tau@tuni.fi](mailto:cris.tau@tuni.fi), and we will remove access to the work immediately and investigate your claim.

# Operating Point Dependent Variable Switching Point Predictive Current Control for PMSM Drives

Sebastian Wendel, *Student Member, IEEE*, Petros Karamanakos, *Senior Member, IEEE*,  
Armin Dietz, Ralph Kennel, *Senior Member, IEEE*

**Abstract**—This contribution presents a direct model predictive current control approach that achieves favorable performance during transients while minimizing the torque and current ripples at steady-state operation by increasing the granularity at which switching can be performed. To meet the control goals, an optimization problem is solved in real-time that decides whether only one discrete voltage space vector or a combination of two is selected. In the latter case, a variable switching point, i.e., a time instant within the control interval at which the converter switches change state, is computed. The proposed method is advantageous, e.g., for electric drives in machine tools, in which, depending on the operating point, fast dynamics and a low torque ripple are important. The approach is evaluated at the example of a two-level voltage source inverter driving a permanent magnet synchronous machine.

**Index Terms**—Variable switching point predictive current control (VSP<sup>2</sup>CC), direct model predictive control (DMPC), finite control set model predictive control (FCS-MPC), SoC FPGA.

## I. INTRODUCTION

The basic principle of finite control set model predictive control (FCS-MPC), also named as direct model predictive control (DMPC), is to find the constrained optimal discrete voltage space vector (SV), which minimizes a pre-defined cost function. By doing so, the control objectives, such as output reference tracking, are met, while very fast transient responses are achieved due to the direct control nature of FCS-MPC. Moreover, when long-horizon FCS-MPC is considered, two features are prominent. First, an improved steady-state system performance can be achieved, as indicated by a reduced total harmonic distortion (THD) of the variables of concern for a given average switching frequency ( $f_{sw}$ ). Second, the stability of the system can be improved.

Nowadays, new and powerful calculation platforms, such as system-on-a-chip field-programmable gate arrays (SoC FPGAs), enable an online calculation of FCS-MPC with a long-horizon up to control frequencies ( $f_c$ ) of several hundred kHz [1]. However, especially for small electric drives with electrical time constants of just a few ms or even  $\mu$ s, the granularity of the switching instants may be still too low for an acceptable torque ripple. Although such a low granularity

might be acceptable during transient operation since a highly dynamic behavior is of greater importance, for steady-state operation it has an adverse effect. Specifically, since one SV is applied to the converter for the whole control interval  $T_c = 1/f_c$ , the theoretical maximum  $f_{sw}$  is limited to half of  $f_c$ . Therefore, the minimization of the torque ripple at steady-state becomes more challenging.

Consequently, a modulator, such as carrier-based pulse width modulation (CB-PWM) or space vector modulation (SVM), seems to be advantageous compared to FCS-MPC, since the state of the converter switch positions can change at any time instant within  $T_c$ . Therefore, owing to the higher granularity of modulator-based schemes, lower torque ripple can be achieved for the same  $f_c$  as with conventional FCS-MPC. Based on the above, it can be concluded that introducing a variable switching point (VSP) (also referred to as switching instant) to FCS-MPC seems meaningful. In doing so, FCS-MPC can apply to the converter more than one SV within one  $T_c$ . Thus, higher switching granularity—and consequently lower torque ripples—can be achieved.

FCS-MPC with two SVs during one  $T_c$  was introduced in, e.g., [2]–[5]. In [2] a so-called variable switching point predictive torque control (VSP<sup>2</sup>TC) and in [3] a variable switching point predictive current control (VSP<sup>2</sup>CC) are presented. However, the approaches in [2], [3], [6]–[8] for VSP<sup>2</sup>TC and VSP<sup>2</sup>CC use only one-step prediction horizon, i.e.,  $N_p = 1$ . Furthermore, in [3] only one transition per  $T_c$  is considered, since a combination of the previous and one new SV is applied. On the contrary, long-horizon VSP<sup>2</sup>CC ( $N_p = 5$ ) is evaluated in [9], showing improved performance of the drive system, but only in simulation. In [4] a so-called modulated MPC (M<sup>2</sup>PC) is introduced. Methods such as [4], [5] solve the optimization problem in two sequential steps, first the optimal SVs are chosen and second their application time is computed. The sequential structure, however, can lead to suboptimal results. Furthermore, strategies such as the one introduced in [10], although achieving fixed  $f_{sw}$  and deterministic harmonic spectra—making them suitable for grid-tied converters—do not exhibit the fast response of FCS-MPC during transients and the resulting three VSPs enforce switching—and switching losses—even if it is unnecessary, e.g., during transients.

However, all previous strategies always apply two (or more) SVs within each control interval. The VSP<sup>2</sup>CC-based method proposed in this paper, however, allows the controller to choose in real-time, based on the cost function, whether a single or two SVs are to be applied within one  $T_c$ . With this

The research leading to these results has received funding from the Bavarian Ministry of Economic Affairs, Energy and Technology and is managed by VDI/VDE under grant agreement ESB048/004. S. Wendel and A. Dietz are with the Institute ELSYS, Technische Hochschule Nuernberg, 90489 Nuremberg, Germany; e-mail: sebastian.wendel@th-nuernberg.de and armin.dietz@th-nuernberg.de. P. Karamanakos is with the Unit of Electrical Engineering, Tampere University, 33101 Tampere, Finland; e-mail: p.karamanakos@ieee.org. R. Kennel is with the Chair of Electrical Drive Systems and Power Electronics, Technical University Munich, 80333 Munich, Germany;

degree of freedom, during transients, the maximum available voltage can be applied to the inverter, either by implementing one active or a combination of two active SVs. At steady-state operation, on the one hand, one active SV can be changed into a zero one (or vice versa) at the computed VSP, thus reducing the current and torque ripples. On the other hand, a zero SV can be applied for the full  $T_c$ . Furthermore, by adopting a two-step horizon ( $N_p = 2$ ) the drive performance is further improved, as indicated by the presented experimental results.

## II. CONTROL MODEL

The proposed VSP<sup>2</sup>CC approach is evaluated with a three-phase two-level voltage source inverter (VSI) and a permanent magnet synchronous machine with surface mounted magnets (SPMSM). The saturation is neglected.

### A. Nonlinear Model of the Drive System

The continuous-time controlled system can be described by (1) and (2) in the dq-frame, where  $R_{ph}$  is the stator resistance,  $L_d$  and  $L_q$  the inductances,  $\Psi_{PM}$  the permanent magnet flux constant,  $\omega_m$  the mechanical angular speed,  $p$  the number of pole pairs.

$$v_d(t) = L_d \frac{di_d(t)}{dt} + R_{ph}i_d(t) - \omega_m(t)pL_qi_q(t) \quad (1)$$

$$v_q(t) = L_q \frac{di_q(t)}{dt} + R_{ph}i_q(t) + \omega_m(t)pL_d i_d(t) + \omega_m(t)p\Psi_{PM} \quad (2)$$

### B. Prediction Model

By discretizing (1) and (2) with forward Euler discretization, the prediction model of the drive is derived, as shown in [1].

$$i_d(k+1) = \frac{T_c}{L_d} (v_d(k) - R_{ph}i_d(k) + \omega_m(k)pL_qi_q(k)) + i_d(k) \quad (3)$$

$$i_q(k+1) = \frac{T_c}{L_q} (v_q(k) - R_{ph}i_q(k) - \omega_m(k)p(L_d i_d(k) + \Psi_{PM})) + i_q(k) \quad (4)$$

Note that the resulting (3) and (4) are also used for the compensation of the delay time—between the time instant the measurements occur and the execution of the control action—caused by the real-time system.

## III. DIRECT MODEL PREDICTIVE CURRENT CONTROL WITH VARIABLE SWITCHING POINT

The proposed controller aims to reduce the current ripples while achieving excellent dynamic behavior. To this end, it decides in real-time whether no switching, one full SV (similar to the classical FCS-MPC) or a VSP with a combination of two SVs is selected. Fig. 1 shows the structure of the algorithm.

### A. Pre-selection Based on the Dead-Beat Control Action

First, a pre-selection method—introduced as “heuristic pre-selection” in [3] and [6]—which utilizes the dead-beat control action is adopted to minimize the computational burden. By doing so, the search space is reduced from eight candidate SVs to three, as shown in, e.g., [3]. More specifically, based on the dead-beat control action, the angle of the desired voltage

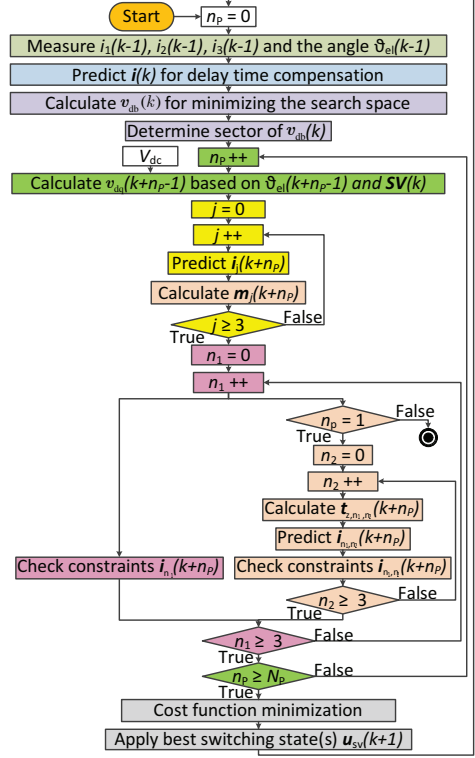


Figure 1. Block diagram of the proposed VSP<sup>2</sup>CC.

vector  $v_{db}(k)$ , that drives the current to its reference, can be calculated based on

$$v_d^*(k) = L_d \frac{i_d^*(k) - i_d(k)}{T_c} + R_{ph}i_d(k) - \omega_m(k)pL_qi_q(k), \quad (5)$$

$$v_q^*(k) = L_q \frac{i_q^*(k) - i_q(k)}{T_c} + R_{ph}i_q(k) + \omega_m(k)pL_d i_d(k) + \omega_m(k)p\Psi_{PM}. \quad (6)$$

$$\gamma(k) = \arctan2(v_q^*(k), v_d^*(k)) + \vartheta_{el}, \{ \gamma \in \mathbb{R} | 0 \leq \gamma < 2\pi \} \quad (7)$$

Using (7), the triangular sector (one out of the six) wherein  $v_{db}(k)$  lies can be determined. Subsequently, the two active SVs and one zero SV that form the sector are selected based on the following principle

$$\mathbf{SV}(k) = \begin{cases} sv_1, sv_2, sv_0/7 & \text{if } 0 \leq \gamma(k) \leq \frac{\pi}{3} & \text{(I)} \\ sv_2, sv_3, sv_0/7 & \text{if } \frac{\pi}{3} < \gamma(k) \leq \frac{2\pi}{3} & \text{(II)} \\ sv_3, sv_4, sv_0/7 & \text{if } \frac{2\pi}{3} < \gamma(k) \leq \pi & \text{(III)} \\ sv_4, sv_5, sv_0/7 & \text{if } \pi < \gamma(k) \leq \frac{4\pi}{3} & \text{(IV)} \\ sv_5, sv_6, sv_0/7 & \text{if } \frac{4\pi}{3} < \gamma(k) \leq \frac{5\pi}{3} & \text{(V)} \\ sv_6, sv_1, sv_0/7 & \text{if } \frac{5\pi}{3} < \gamma(k) \leq 2\pi & \text{(VI)}. \end{cases} \quad (8)$$

Thus, only these three SVs are candidate solutions for the subsequent MPC problem. Moreover, to reduce the switching frequency (and thus switching losses) the zero SV ( $sv_0$  or  $sv_7$ ) that results in less switching effort—with respect to the previously applied SV—is considered. Finally, it is worth mentioning that even though there is a possibility that the reduction of the search space based on the location of the dead-beat control action on the plane can lead to suboptimal

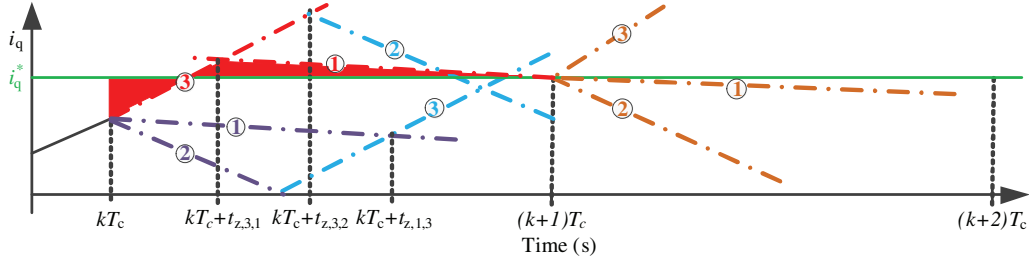


Figure 2. Variable switching points by the intersection of two  $i_q$  current trajectories for  $N_p=2$ .

results, the simulation and experimental results based on the chosen case study do not show any suboptimal performance.

### B. Proposed VSP<sup>2</sup>CC Concept

The proposed algorithm evaluates a horizon of  $N_p$  steps by calculating the stator currents for different combinations of the three candidate SVs based on (3) and (4). For the first prediction step, the three candidate SVs are evaluated by taking into account two possibilities: either one SV is applied to the inverter for the whole  $T_c$  (i.e., akin to the conventional FCS-MPC), or two SVs are executed within one  $T_c$  according to the principles of VSP<sup>2</sup>CC. For the prediction steps further in the horizon, i.e.,  $N_p > 1$ , the algorithm theoretically has the ability to evaluate all the possible SV combinations by employing the VSP<sup>2</sup>CC concept (nine in total). This implies that two SVs can be applied in each prediction step. By doing so, nonetheless, the possible solutions to be enumerated are  $3^{2N_p}$ , i.e., the optimization problem can become computationally intractable for  $N_p > 1$ . To overcome this issue, the concept of standard FCS-MPC is employed for steps  $N_p > 1$ , meaning that only three candidate solutions are considered from the second step of the horizon onwards, see the light red calculations on the right-hand side of Fig. 1. As a result, the MPC algorithm has to evaluate only  $3^{N_p+1}$  possible solutions in total. As can be understood, the aforementioned simplification greatly reduces the computational complexity, thus facilitating its real-time implementation. Finally, it should be stressed out, that owing to the receding horizon, only the first element (i.e., control action) of the solution is implemented. From a performance point of view, this means that the first step of the horizon is the one with the greatest significance. Hence, adopting the standard FCS-MPC for  $N_p > 1$  does not adversely affect the system performance.

To decide which SVs meet the control objectives, as mentioned in the beginning of this section, the slopes of  $i_d$  and  $i_q$  are calculated. Before doing so, the following assumptions are made:

- The saturation does not affect the slopes during one period  $T_c$ . Therefore, the slopes are supposed to be linear. However, in case the used SPMSM has a noticeable saturation effect during one  $T_c$  (i.e.,  $10\mu\text{s}$ ), this assumption is dropped, and the adopted approach needs to be refined.
- The rotor angle  $\vartheta_{el}$  is kept constant during one period  $T_c$ . However, for machines with many pole pairs when operated at high speed, the slopes change during one  $T_c$ . For example, when  $n_m = 4000\text{ rpm}$ ,  $p = 4$  and  $T_c =$

$10\mu\text{s}$ ,  $\vartheta_{el}$  can change around  $0.01657\text{ rad}$ , which can lead to a voltage error of  $1.8\%$ .

- Non-linear time-varying parameters, such as  $R_{ph}$ ,  $\Psi_{PM}$  and the state  $\omega_m$  have significantly bigger time constants. Therefore, their variation does not affect the slope of the currents over one  $T_c$ .

By assuming constant current slopes for the entire period  $T_c$ , as seen in [7]–[9], (9) computes the slope of the resulting current trajectory for each of the three SVs.

$$\mathbf{m}_{dq}(k) = \frac{\mathbf{i}_{dq}(k+1) - \mathbf{i}_{dq}(k)}{T_c} = \frac{\Delta \mathbf{i}_{dq}(k)}{T_c} \quad (9)$$

Taking the previous assumptions into account, the same slopes are assumed at time steps  $k$  and  $k+1$ . By denoting these slopes with the subscripts  $n_1$  and  $n_2$ , respectively, the rms current error on the d- and q-axis can be calculated over the whole period  $T_c$  with (10) [3], [6].

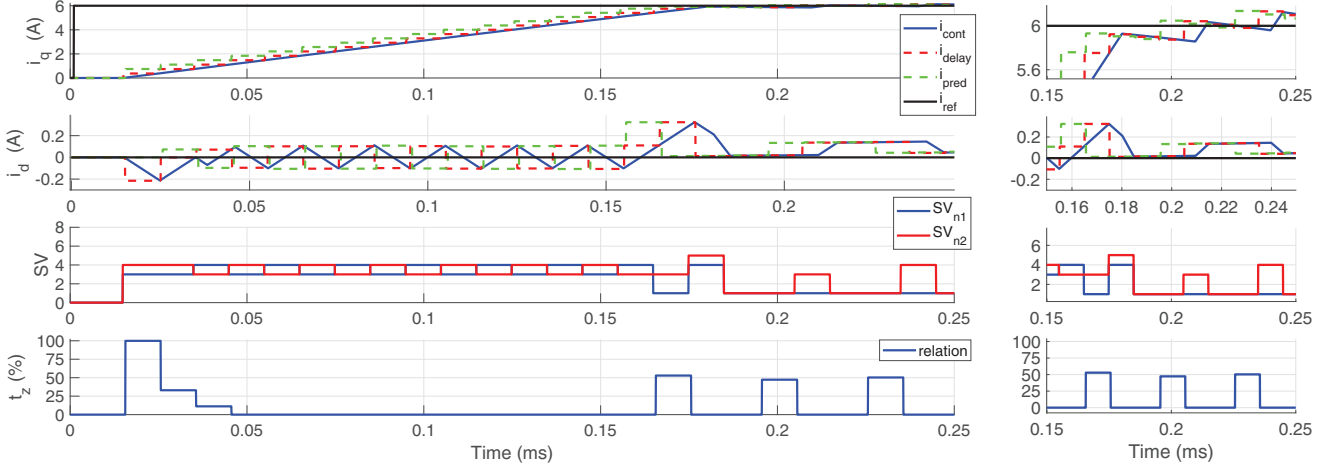
$$\begin{aligned} e_{\text{rms}^2, n_1, n_2}(t) = & \frac{1}{T_c} \left( \int_0^{t_{z, n_1, n_2}} (i_d + m_{d, n_1} t - i_d^*)^2 dt \right. \\ & + \int_{t_{z, n_1, n_2}}^{T_c} (i_d + m_{d, n_2} t - i_d^*)^2 dt \\ & + \int_0^{t_{z, n_1, n_2}} (i_q + m_{q, n_1} t - i_q^*)^2 dt \\ & \left. + \int_{t_{z, n_1, n_2}}^{T_c} (i_q + m_{q, n_2} t - i_q^*)^2 dt \right) \end{aligned} \quad (10)$$

An illustrative example of the resulting error area (in red) is shown in Fig. 2 with a combination of  $sv_3$  and  $sv_1$  for  $i_q$ . Expression (10) is calculated for each SV combination including the single SVs as shown in Fig. 1. The variable switching point  $t_{z, n_1, n_2}$ , which minimizes the current ripple for each SV combination, can be obtained by setting the derivative of (10) to zero, i.e.,  $de_{\text{rms}^2}/dt_z = 0$ . This yields

$$t_{z, n_1, n_2} = \frac{a_{n_1, n_2} + b_{n_1, n_2}}{c_{n_1, n_2} + d_{n_1, n_2}} \quad \text{where} \quad (11)$$

$$\begin{aligned} a_{n_1, n_2} &= (m_{d, n_2} - m_{d, n_1})(2i_d - 2i_d^* + T_c m_{d, n_2}), \\ b_{n_1, n_2} &= (m_{q, n_2} - m_{q, n_1})(2i_q - 2i_q^* + T_c m_{q, n_2}), \\ c_{n_1, n_2} &= (m_{d, n_1} - m_{d, n_2})(2m_{d, n_1} - m_{d, n_2}), \\ d_{n_1, n_2} &= (m_{q, n_1} - m_{q, n_2})(2m_{q, n_1} - m_{q, n_2}). \end{aligned}$$

To further simplify the calculation of  $t_{z, n_1, n_2}$ , so as to alleviate the associated computational effort, (9) is utilized. This is advantageous for the subsequent implementation (especially in fixed point) on an FPGA, as described in Section V. In doing so,  $T_c$  is set as a common factor, whereat the range of the values  $t_{z, n_1, n_2}$  is reduced considerably, resulting in



(a) Reference current step from  $i_q^* = 0$  A to  $i_q^* = 6$  A.

(b) Close-up view.

Figure 3. Simulation: Reference current step and the the resulting voltage space vectors for  $i_q^*$  with  $i_d^* = 0$  A by using VSP<sup>2</sup>CC with  $\lambda_u = 0.2$ .

$$t_{z,n_1,n_2} = T_c \frac{a_{n_1,n_2} + b_{n_1,n_2}}{c_{n_1,n_2} + d_{n_1,n_2}} \quad \text{where} \quad (12)$$

$$\begin{aligned} a_{n_1,n_2} &= (\Delta i_{d,n_2} - \Delta i_{d,n_1})(2i_d - 2i_d^* + \Delta i_{d,n_2}), \\ b_{n_1,n_2} &= (\Delta i_{q,n_2} - \Delta i_{q,n_1})(2i_q - 2i_q^* + \Delta i_{q,n_2}), \\ c_{n_1,n_2} &= (\Delta i_{d,n_1} - \Delta i_{d,n_2})(2\Delta i_{d,n_1} - \Delta i_{d,n_2}), \\ d_{n_1,n_2} &= (\Delta i_{q,n_1} - \Delta i_{q,n_2})(2\Delta i_{q,n_1} - \Delta i_{q,n_2}). \end{aligned}$$

Observing (12), it is evident that when the SVs at  $k$  and  $k+1$  are equal, the same current slope is considered over the whole  $T_c$  resulting in a switching time of  $t_{z,n_1,n_2} = 0$ . In this case, the chosen SV will be applied for the full period  $T_c$ . By doing so, only one switching transition occurs within  $T_c$ , or when the previously applied SV is the same, then switching is avoided altogether. Furthermore, SV combinations that result in current trajectories that do not intersect at all within  $T_c$ , or lead to  $t_{z,n_1,n_2} > T_c$  are excluded as infeasible.

### C. Optimization Problem

The cost function decides if only one SV, a combination of two of them or no switching at all is applied, based on

$$\begin{aligned} J_f(k) &= \sum_{l=k}^{k+N_p-1} |\hat{i}_{q,t_z}(l+1) - i_q^*(k)| + |\hat{i}_{q,T_c}(l+1) - i_q^*(k)| \\ &\quad + |\hat{i}_{d,t_z}(l+1) - i_d^*(k)| + |\hat{i}_{d,T_c}(l+1) - i_d^*(k)| \\ &\quad + \hat{f}(i_{dq}(l+1)) + \lambda_u \Delta U(l). \end{aligned} \quad (13)$$

$$\hat{f}(i_{dq}(l+1)) = \begin{cases} 4 & \text{if } |i_d(l+1)| + |i_q(l+1)| > i_{\max} \\ 0 & \text{if } |i_d(l+1)| + |i_q(l+1)| \leq i_{\max} \end{cases} \quad (14)$$

For computing the optimal SV(s), the predicted currents are inserted in (13) by taking into account the hard constraint (14), where “4” is the maximum current in per unit (p.u.)<sup>1</sup>. The cost function takes into account that either two SVs, or

one SV can be applied. In the former case, the algorithm uses the pair of SVs and the corresponding current errors of  $i_q$  and  $i_d$  are calculated at time instants  $t_z$  and  $T_c$ . In the latter case, due to  $t_z = 0$ , the first current term of (13) for  $i_d$  and  $i_q$  uses the same current error as the second term at  $T_c$  in order to enable a comparable cost. Moreover, the term  $\Delta U$  is used to penalize switching transitions. By adjusting the weighting factor  $\lambda_u \geq 0$  the average switching frequency can be lowered (at the expense of higher current ripples). In this work,  $\lambda_u = 0$  for the standard FCS-MPC, while  $\lambda_u > 0$  for the VSP<sup>2</sup>CC so that a comparison—in terms of current THD and ripple—between the two methods at almost equal average  $f_{sw}$  is possible.

## IV. SIMULATION RESULTS

Fig. 3 shows the simulation results for  $i_d$  and  $i_q$  during start up with the parameters from Table I with  $f_{sw} \approx 15$  kHz ( $\lambda_u = 0.2$ ). As can be seen, the algorithm decides at the beginning to use only one active SV to achieve an as fast response as possible. For  $\lambda_u = 0$ , two active SVs during one  $T_c$  would be applied to reduce the current ripple in the d-axis. In the same figure the application time of  $SV_{n1}$  is also shown as percentage of  $T_c$  for each discrete time step. As observed, in steady-state operation, the ripple is minimized by using two SVs (one active and one zero) or by applying just a single zero SV. This case occurs, e.g., for  $t < 0.165$  ms, where a zero SV is applied consecutively for several full periods until  $t = 0.165$  ms. In the period, starting at this instant, two SVs are applied; first a zero vector, followed by an active one. As a result, the number of switching transitions is minimized while keeping the current ripple acceptable.

## V. EXPERIMENTAL RESULTS

The proposed algorithm is implemented on the FPGA of a Zynq-7000 (XC7Z020) SoC, which is shown in Fig. 4, via the HDL-Coder from MathWorks, as introduced in [1]. The processor is used for the parametrization of the MPC

<sup>1</sup>Theoretically, a soft constraint is to be preferred since it can avoid feasibility problems when solving (13).



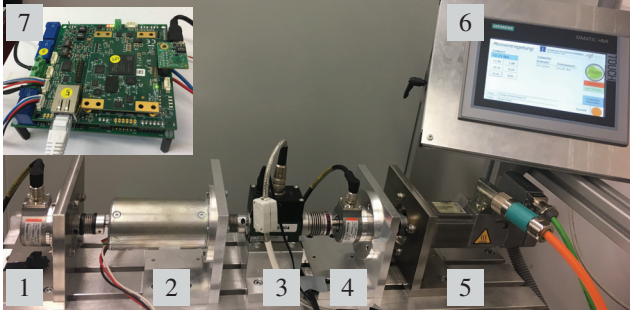


Figure 4. Test bench - (1) motor speed encoder, (2) test motor (SPMSM), (3) torque measuring shaft, (4) load speed encoder, (5) load machine, (6) HMI for the load machine, (7) SoC platform, combined with the VSI.

algorithm (i.e.  $R_{ph}$ ,  $L$  or  $\lambda_u$ ) and the communication. So far, all previous VSP<sup>2</sup>C(T)C methods [2], [3], [6]–[9] were only on a simulation level or implemented on the processor. In contrast to Fig. 4, a shunt measurement is used instead of the the fluxgate current sensors, since these inherently exhibit oscillations at high sampling frequencies. The FPGA implementation is advantageous, since high clock frequencies (e.g. 100 MHz) can be used for both parallel and serial calculations. This enables high sampling and calculation frequencies for long prediction horizons. As described in [1], the algorithm is parallelized when possible, and implemented in serial only when necessary. Furthermore, for an efficient implementation, resource streaming is used for the for-loops and the fixed point value range is chosen based on a normalized (i.e., p.u.) scaling. So far, a floating point implementation of the algorithm on the FPGA is not efficient. In addition, since divisions are not really efficient in real-time at all (and especially with FPGAs), the bit size and fixed point value range of the required division in (12) is kept as small as possible.

Table I  
MOTOR AND SYSTEM PARAMETERS

Description	Symbol	Value	Unit
Rated torque	$T_N$	47	Ncm
Winding resistance	$R_{ph}$	0.07	$\Omega$
Winding inductance	$L_{ph} = L_d = L_q$	0.375	mH
Voltage constant	$k_u$	6.6	mV/rpm
Pole pair number	$p$	4	
DC link voltage	$V_{dc}$	24	V
Sampling and control frequency	$f_c$	100	kHz

#### A. Current Measurements

Figs. 5(a)–(b) and Fig. 5(c) show the phase current and phase current ripple for VSP<sup>2</sup>CC with dead-beat pre-selection and standard FCS-MPC, respectively, when a reference current of  $i_q^* = 6$  A and  $i_d^* = 0$  A at  $n_m = 450$  rpm with  $N_p = 2$  are concerned. Figs. 7–8 show the phase current with  $i_q^* = 1$  A and  $i_d^* = 0$  A at  $n_m = 200$  rpm for FCS-MPC and VSP<sup>2</sup>CC with  $N_p = 2$ , respectively. As expected, FCS-MPC and VSP<sup>2</sup>CC have slightly different average  $f_{sw}$  and thereby produce different current ripples depending on the operating point. Therefore, in the case of VSP<sup>2</sup>CC,  $\lambda_u$  is increased to achieve a comparison between standard FCS-MPC and VSP<sup>2</sup>CC at an almost equal average  $f_{sw}$ , shown in Table II. Moreover, Figs. 7–8 show, that for an almost equal average  $f_{sw}$ , a reduced current

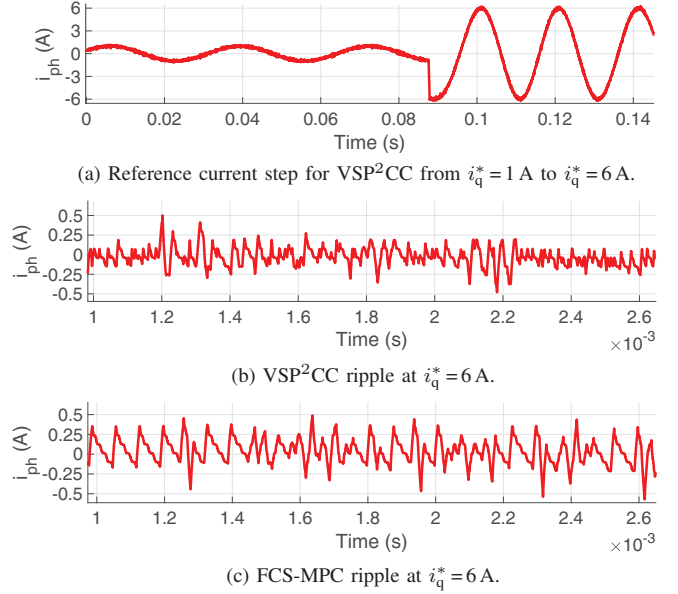


Figure 5. Single-phase stator current for VSP<sup>2</sup>CC with  $\lambda_u = 0.2$ ,  $f_{sw} = 21$  kHz and FCS-MPC with  $f_{sw} = 20$  kHz at  $n_m = 450$  rpm.

ripple and lower current THD can be achieved with VSP<sup>2</sup>CC. The spectrum of the VSP<sup>2</sup>CC approach is shown in Fig. 6, as calculated over 20 fundamental periods. It is expected to achieve much better results once oversampling is used for the current measurement, since the measurement accuracy has a strong impact.

Table II  
THD FOR FCS-MPC AND VSP<sup>2</sup>CC

$N_p = 2$	avg. $f_{sw}$	THD	$n_m$	$i_q^*$
FCS-MPC	24 kHz	3.3 %	1520 rpm	6 A
$\lambda_u = 0.0$	38 kHz	2.31 %	1520 rpm	6 A
$\lambda_u = 0.1$	31 kHz	2.69 %	1520 rpm	6 A
FCS-MPC	22 kHz	2.5 %	720 rpm	6 A
$\lambda_u = 0.0$	37 kHz	1.43 %	720 rpm	6 A
$\lambda_u = 0.1$	26 kHz	1.72 %	720 rpm	6 A
$\lambda_u = 0.2$	22 kHz	2.01 %	720 rpm	6 A
FCS-MPC	20 kHz	3.13 %	450 rpm	6 A
$\lambda_u = 0.0$	38 kHz	2.07 %	450 rpm	6 A
$\lambda_u = 0.1$	26 kHz	2.08 %	450 rpm	6 A
$\lambda_u = 0.2$	21 kHz	2.29 %	450 rpm	6 A
FCS-MPC	15 kHz	11 %	200 rpm	1 A
$\lambda_u = 0.0$	34 kHz	3.2 %	200 rpm	1 A
$\lambda_u = 0.1$	19 kHz	6.59 %	200 rpm	1 A
$\lambda_u = 0.2$	14 kHz	7.88 %	200 rpm	1 A

In general, at high speed or for high reference currents (in contrast to low speed and/or for small reference currents) a higher voltage margin is required. This implies that with direct MPC (FCS-MPC and VSP<sup>2</sup>CC), more active SVs are used, whereas zero SVs are less frequently utilized. The other way

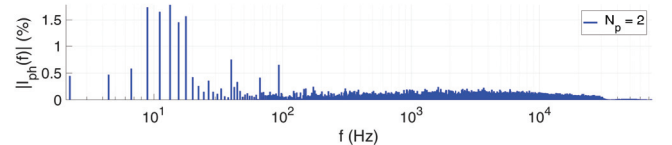


Figure 6. Current spectrum of VSP<sup>2</sup>CC with  $\lambda_u = 0.2$  for  $i_q^* = 1.0$  A.

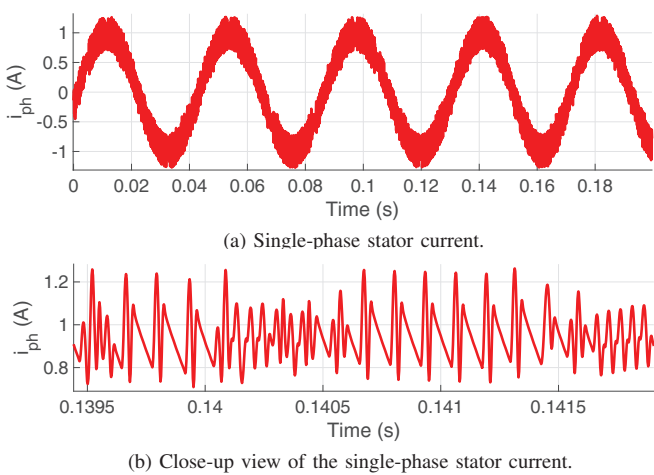


Figure 7. Single-phase stator current for FCS-MPC with  $f_{sw} = 15.8$  kHz at  $n_m = 200$  rpm.

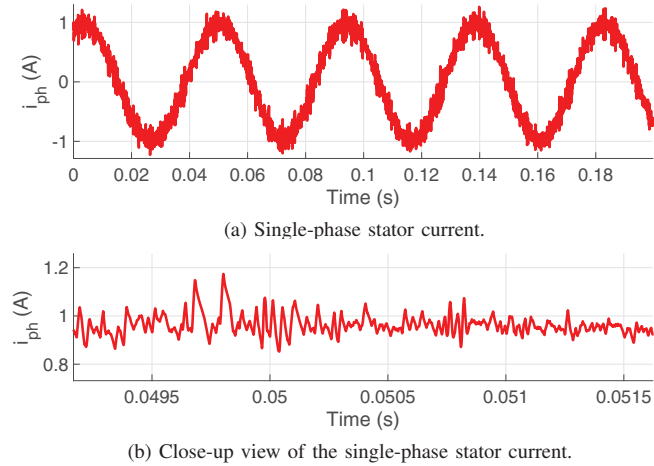


Figure 8. Single-phase stator current for VSP<sup>2</sup>CC with  $\lambda_u = 0.2$ ,  $f_{sw} = 14.3$  kHz at  $n_m = 200$  rpm.

around, for low speeds and/or small  $i^*$ , where zero vectors are mostly used, the advantage of VSP<sup>2</sup>CC is obvious, since a VSP, i.e., a time instant within the control interval at which the converter switches change, is chosen. This effect is apparent in Fig. 9. In addition, it has to be mentioned, that the current slopes are minimal steeper at increased speed and currents.

### B. Resource and Timing Evaluation

Tab. III shows the required total resources and the achieved timing when implementing the algorithm on an FPGA with a clock frequency of 100 MHz. Even if the resources depend on the specific way of implementation (sharing and streaming), the provided information is useful since it can indicate the required resources and/or computational load for an increased horizon or more complex cost functions.

Table III  
RESOURCE AND TIMING EVALUATION FOR  $N_p = 2$

Resources	LUTs	Block RAMs	Flip-Flops	DSP-Slices	
	28804	38	28337	126	
Total timing	Sampling	Dead-Beat	Prediction	Optimization	
	3.4 $\mu$ s	1.0 $\mu$ s	0.2 $\mu$ s	2.16 $\mu$ s	0.04 $\mu$ s

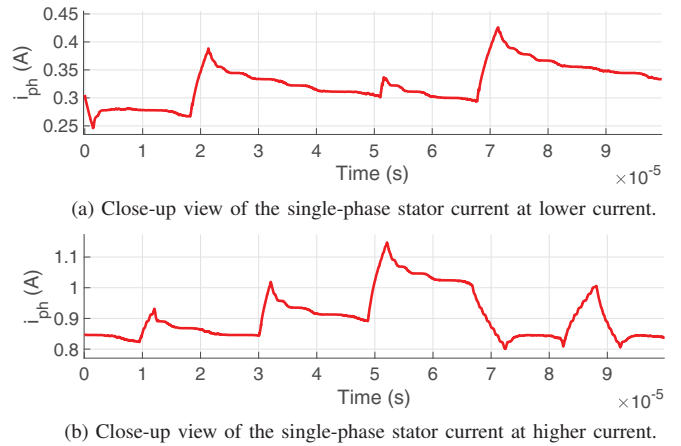


Figure 9. Single-phase stator current for VSP<sup>2</sup>CC with  $\lambda_u = 0.1$ ,  $f_{sw} = 19$  kHz at  $n_m = 200$  rpm.

## VI. CONCLUSION

The presented VSP<sup>2</sup>CC algorithm enables a high granularity for the switching instants. Thus it can significantly reduce the current ripple, and thereby indirectly the torque ripple depending on the operating point. Moreover, it comes with all FCS-MPC advantages, such as direct consideration of constraints, or the possibility to apply only active SVs during transients. The latter allows for the fastest possible dynamic operation of the drive, limited only by the available DC link voltage margin. Future work includes the comparison of the proposed VSP<sup>2</sup>CC approach with field oriented control (FOC) with SVM. Furthermore, longer horizons, the impact of parameter inaccuracy, and current oversampling for higher accuracy will be evaluated in detail.

## REFERENCES

- [1] S. Wendel, et al., "FPGA Based Finite-Set Model Predictive Current Control for Small PMSM Drives With Efficient Resource Streaming," *4th Symp. on Pred. Control of Elect. Drives and Power Elec.*, Sep. 2017.
- [2] P. Karamanakos, "Model Predictive Control Strategies for Power Electronics Converters and AC Drives," *PhD Thesis*, July 2013.
- [3] P. Stolze, et al., "Heuristic Variable Switching Point Predictive Current Control for the Three-Level Neutral Point Clamped Inverter," *IEEE Int. Symp. on Sensorless Control for Elect. Drives and Pred. Control of Elect. Drives and Power Elec.*, Oct. 2013.
- [4] L. Tarisciotti, et al., "Modulated Model Predictive Control for a Three-Phase Active Rectifier," *IEEE Trans. On Ind. Appl.*, Vol. 51, No. 2, p. 1610-1620, 2015.
- [5] Y. Zhang, et al., "Low-Complexity Model Predictive Power Control: Double-Vector-Based Approach," *IEEE Trans. On Ind. Elec.*, Vol. 61, No. 11, p. 5871-5880, 2014.
- [6] P. Stolze, et al., "Effective variable switching point predictive current control for ac low-voltage drives," *Int. Journ. of Control*, Vol. 88, No. 7, p. 1366-1378, 2015.
- [7] P. Karamanakos, et al., "Variable Switching Point Predictive Torque Control of Induction Machines," *IEEE Journ. of Emerging and Selected Topics in Power Elec.*, Vol. 2, No. 2, June 2014.
- [8] P. Karamanakos, et al., "A Variable Switching Point Predictive Current Control Strategy for Quasi-Z-Source Inverters," *IEEE Trans. On Ind. Appl.*, Vol. 54, No. 2, Apr. 2018.
- [9] I. Alevras, et al., "Variable Switching Point Predictive Torque Control With Extended Prediction Horizon," *IEEE Int. Conf. on Ind. Technology (ICIT)*, March 2015.
- [10] P. Karamanakos, et al., "Fixed Switching Frequency DIRECT Model Predictive Control Based on Output Current Gradients," *IECON - 44th Annual Conf. of the IEEE Ind. Elec. Society*, Oct. 2018.